

## A Measurement of the Ratio of the $W + 1$ Jet to $Z + 1$ Jet Cross Sections with ATLAS

A. Meade and B. Brau on behalf of the ATLAS Collaboration  
 Department of Physics, University of Massachusetts, Amherst, MA, USA

The measurement of hadronic activity recoiling against  $W$  and  $Z$  vector bosons provides an important test of perturbative QCD, as well as a method of searching for new physics in a model independent fashion. We present a study of the cross-section ratio for the production of  $W$  and  $Z$  gauge bosons in association with exactly one jet  $R_{\text{jet}} = \sigma(W + 1\text{jet})/\sigma(Z + 1\text{jet})$ , in  $pp$  collisions at  $\sqrt{s} = 7$  TeV. The study is performed in the electron and muon channels with data collected with the ATLAS detector at the LHC. The ratio  $R_{\text{jet}}$  is studied as a function of the cumulative transverse momentum distribution of the jet. This result can be compared to NLO pQCD calculations and the prediction from LO matrix element + parton shower generators.

### I. INTRODUCTION

Measurements of the cross sections of the  $W$  and  $Z$  bosons in association with hadronic activity are important tests of the standard model, particularly perturbative quantum chromodynamics. In addition many searches for models of physics beyond the Standard Model have significant  $W$ +jets or  $Z$ +jets backgrounds, adding to the importance of understanding these processes. Individual measurements of  $W$  or  $Z$  cross sections in association with jets are limited by systematics that are shared between the two measurements, such as the luminosity and the jet energy scale. In contrast, in measurements of the ratio between  $W$  and  $Z$  cross sections, many of these uncertainties cancel due to the similar nature of  $W$  and  $Z$  production. For this reason the  $W/Z$  cross section ratio can be the basis for a program of high precision measurements.

This study reports on a measurement of the ratio of production cross sections of the  $W$  and  $Z$  bosons with exactly one associated jet with  $p_T > 30$  GeV as a function of jet transverse momentum threshold. This binning implies that each bin contains all events with a jet above the threshold. The data for this analysis consists of the entire 2010 ATLAS dataset, operating at the Large Hadron Collider (LHC). This corresponds to  $33 \text{ pb}^{-1}$  of integrated luminosity, taken at a center of mass energy of 7 TeV. A paper on this measurement has been produced by the ATLAS collaboration [1].

The ratio is measured in a fiducial measurement volume of the detector where the leptons and jets are measured with good resolution, in order to avoid theoretical uncertainties associated with modeling particles outside of the detector volume. The fiducial region is defined by the following kinematic ranges of the lepton(s)  $\ell$ , neutrino  $\nu$ , and jet:  $p_T^\ell > 20$  GeV,  $p_T^\nu > 25$  GeV,  $p_T^{\text{jet}} > 30$  GeV,  $|\eta^{\text{jet}}| < 2.8$ . The electrons and muons were restricted to different pseudorapidity ranges, for electrons  $1.52 < |\eta| < 2.47$  or  $|\eta| < 1.37$ , while for muons  $|\eta| < 2.4$ . For the  $W$ , the transverse mass, defined as  $m_T = \sqrt{2p_T^\ell p_T^\nu (1 - \cos(\phi^\ell - \phi^\nu))}$  was required to satisfy  $m_T > 40$  GeV. The dilepton invariant mass of the  $Z$  was required to be within the range  $71 < m_{\ell\ell} < 111$  GeV.

Particle level jets were defined as jets reconstructed in simulated events by applying the anti- $k_t$  jet reconstruction algorithm [2] with a radius parameter  $R = 0.4$  to all final state particles with a lifetime longer than 10 ps (including muons and non-interacting particles). Particle level electrons were defined by including the energy of all radiated photons within a cone of  $\Delta R = 0.1$  around each electron (with  $\Delta R = \sqrt{(\Delta\eta)^2 + (\Delta\phi)^2}$ ). In the muon case the “bare” final state muon is taken as the particle level muon, with no radiated photons included.

### II. THE ATLAS DETECTOR

The ATLAS detector is described in detail elsewhere [3]. Immediately surrounding the interaction point is the inner detector (ID), providing precision tracking and vertexing capabilities, surrounded by a large solenoidal magnet. Outside of this volume lies the electromagnetic and hadronic calorimeters, used for energy measurement and electron and photon identification. The outermost portion of the detector is the muon spectrometer (MS), based on three large superconducting toroids and a system of three stations of trigger chambers and precision tracking chambers.

arXiv:1110.0435v1 [hep-ex] 3 Oct 2011

### III. SIMULATED EVENT SAMPLES

Simulated event samples were used to correct signal yields for detector effects, for some of the background estimates, and for comparison of the results to theoretical expectations. Samples of  $W \rightarrow \ell\nu + N_{\text{parton}}$  and  $Z \rightarrow \ell\ell + N_{\text{parton}}$  (where  $\ell = e, \mu, \tau$ ) were generated using ALPGEN [4]. Background and additional signal samples were generated with PYTHIA [5] and POWHEG [6]. To take into account overlapping pp collisions some samples were generated with multiple non-diffractive scattering events overlapping with the primary collision event. These samples were reweighted such that the distribution of the number of reconstructed primary vertices matched that of the data sample. GEANT4 [7] was used to simulate the detector response for all samples, and these samples were subject to the same reconstruction and analysis chain as the  $pp$  collision data.

Predictions for the  $W$  and  $Z$  cross sections as a function of jet  $p_T$  threshold at NLO were obtained using MCFM, with corrections to particle level calculated using PYTHIA, to account for initial and final state radiation, hadronization, and underlying event.

### IV. DATA AND EVENT SELECTION

Kinematic requirements for reconstructed muon and electron candidates match those of the fiducial definition:  $p_T > 25$  GeV,  $|\eta| < 2.4$ . In the electron channel events were triggered based on the presence of an electromagnetic cluster with  $E_T > 15$  GeV. Electron candidates were required to satisfy lateral shower containment, shape and width criteria, and minimal leakage into the hadronic calorimeter in order to be classified as “medium”. Consistency between track  $p_T$  and cluster energy as well as tighter hit requirements are additionally required to categorize an electron as “tight”. For the electron channel the pseudorapidity range region  $1.37 < |\eta| < 1.51$  is rejected due to a gap in the calorimeter coverage.

In the muon channel, events were selected by the trigger based on muon spectrometer hits consistent with a track of 10 or 13 GeV, the tighter requirement applying to later data with higher instantaneous luminosity. Muon candidates were required to have inner detector and muon spectrometer tracks and pass kinematic requirements to be classified as “medium”. To be classified as “tight,” consistency is demanded between ID and MS track, and requirements on the number of inner detector hits were made. In addition, the impact parameters of the muon are required to be consistent with the interaction point, and the inner detector track is required to be isolated from other energetic tracks, with  $\sum p_T$  of all tracks within  $\Delta R < 0.2$  less than 1.8 GeV.

Each event was required to have a reconstructed primary vertex with three or more tracks, and to be within 150 mm of the center of the detector along the beamline.  $W$  candidates were required to have exactly one “tight” lepton with no additional “medium” leptons,  $E_T^{\text{miss}} > 25$  GeV, and  $M_T > 40$  GeV.  $Z$  candidates are required to have exactly two leptons of opposite charge, one “tight”, and one of “medium” or higher quality. The invariant mass  $m_{\ell\ell}$  of the lepton pair is required to be in the range  $71 < m_{\ell\ell} < 111$  GeV.

Reconstructed jets were defined using the anti- $k_t$  jet reconstruction algorithm with a radius parameter  $R = 0.4$  as in the fiducial definition. These jets were required to be within the kinematic range  $p_T > 30$  GeV,  $|\eta| < 2.8$ . Events were rejected if identified as likely to contain a jet from detector noise or a cosmic ray. Events with jets within a cone of  $\Delta R < 0.6$  from an electron are rejected to avoid distortion of the shower shape from the nearby electromagnetic shower, which could result in reconstruction inefficiency or incorrect energy measurement. Jets from additional interactions in a bunch crossing were rejected by requiring that 75% of the scalar sum  $p_T$  of all tracks associated with a jet came from tracks originating from the same primary vertex. This approach is termed the jet vertex fraction (JVF) algorithm. Only events containing exactly one jet passing these requirements were selected as candidate events.

Using these  $W(Z)$  selection criteria, 12112 (948) events and 12995 (1376) events were found in the electron and muon channels respectively.

### V. BACKGROUND ESTIMATION

Backgrounds to the measurement are determined independently for each bin of the measurement in jet  $p_T$  threshold. These backgrounds are categorized as resulting from electroweak or QCD multijet processes, and are subtracted from the total number of events passing selection using the following formula to obtain the signal event yield  $N_{\text{sig}}$ :

$$N_{\text{sig}} = N_{\text{tot}} \cdot (1 - f_{\text{multijet}})(1 - f_{\text{ewk}}) \quad (1)$$

The predicted number of events passing selection cuts is shown for all signal and background processes in Table I.

The electroweak background fraction  $f_{\text{ewk}}$  is estimated from simulated data as a fraction of the total multijet subtracted event count. This has the advantage of having no dependence on the luminosity, and reduces dependence of the background on our measurement volume, as the electroweak processes have similar kinematic distributions.

The multijet background processes are estimated using data driven methods that vary based on the channel. In the  $W \rightarrow e\nu$  channel, signal and background templates were fit to the control region  $15 \text{ GeV} < E_{\text{T}}^{\text{miss}} < 55 \text{ GeV}$  to determine the background fraction. The signal and electroweak background template shapes are taken from simulation. The multijet event shapes are found from data by selecting “medium” electron candidates and requiring that 2 of the “tight” selection requirements, as well as isolation, are failed, producing what is essentially an electron-like multijet sample. The  $Z \rightarrow ee$  background estimate was performed using a similar method by fitting templates to the dilepton invariant mass spectrum. Because of smaller background, a looser electron selection and reversal of two of the “medium” selection criteria were used in the determination of the multijet template.

In the  $W \rightarrow \mu\nu$  channel, the multijet background is estimated by measuring the number of events passing all selection, and all selection but isolation. The efficiency of this selection is then measured on data control samples in the data. Dimuon events from  $Z$  events are used to measure the efficiency for muons from electroweak processes like the  $W$  and  $Z$  signal, and dijet events are used to measure the efficiency for muons from the multijet background. Since these two efficiencies are significantly different, the multijet background fraction can be determined. In the  $Z \rightarrow \mu\mu$  channel, the multijet background is very small. In this case a scale factor is derived by comparing non-isolated dimuon pairs in data and simulation, and used to normalize a simulated multijet sample.

In the electron  $W$  channel, multijet backgrounds are the dominant background due to the relatively high probability of a jet fragmentation product being reconstructed as an electron. The electron multijet background fraction was about 16% for the lowest jet threshold, 30 GeV.  $Z \rightarrow ee$ ,  $W \rightarrow \tau\nu$ , and  $t\bar{t}$  events are all significant sources of electroweak background, which is around 3.4%. The dominant backgrounds in the  $W \rightarrow \mu\nu$  channel are  $W \rightarrow \tau\nu$  decaying to a muon (2%),  $Z \rightarrow \mu\mu$  with one muon failing to be reconstructed (3%), and multijet events (3%). In both the electron and muon  $Z$  channels, backgrounds were very small, less than 1% for all  $Z$  candidates.

Process	$W \rightarrow e\nu$	$Z \rightarrow ee$	Process	$W \rightarrow \mu\nu$	$Z \rightarrow \mu\mu$
$W \rightarrow e\nu$	$9340 \pm 40$	$3 \pm 1$	$W \rightarrow \mu\nu$	$11860 \pm 40$	$4 \pm 2$
$Z \rightarrow ee$	$106 \pm 3$	$880 \pm 10$	$Z \rightarrow \mu\mu$	$360 \pm 6$	$1370 \pm 40$
$W \rightarrow \tau\nu$	$191 \pm 6$	$0.2 \pm 0.2$	$W \rightarrow \tau\nu$	$234 \pm 6$	$0.3 \pm 0.6$
$t\bar{t}$	$33 \pm 1$	$1.9 \pm 0.2$	$t\bar{t}$	$35 \pm 1$	$3 \pm 2$
$Z \rightarrow \tau\tau$	$19 \pm 1$	$0.3 \pm 0.1$	$Z \rightarrow \tau\tau$	$22 \pm 1$	$0.3 \pm 0.6$
Multijet	$1800 \pm 60$	$2.9 \pm 0.6$	Multijet	$380 \pm 70$	$4 \pm 4$
Other	$58 \pm 2$	$1.1 \pm 0.1$	Other	$117 \pm 1$	$8 \pm 3$
Total	$11550 \pm 70$	$880 \pm 10$	Total	$13010 \pm 80$	$1380 \pm 40$
Data $N_{\text{tot}}$	12112	948	Data $N_{\text{tot}}$	12995	1376

TABLE I: Predicted and observed events in data in the electron and muon channels for the  $W$  and  $Z$  selections for  $\int \mathcal{L} dt = 33 \text{ pb}^{-1}$ . Background estimates are quoted for a jet  $p_T$  threshold of 30 GeV. Only statistical errors are displayed. “Other” includes contributions from diboson and single top events.

## VI. CORRECTION PROCEDURE

Event yields were corrected for trigger efficiency ( $\epsilon_{\text{trig}}^\ell$ ), lepton identification efficiency ( $\epsilon^\ell$ ), and differences between boson acceptance at detector level ( $A_{\text{reco}}$ ) and particle level ( $A_{\text{part}}$ ) due to resolution effects ( $C_V^\ell = \frac{A_{\text{reco}}}{A_{\text{part}}}$ ). The number of signal events for each boson at particle level was then obtained using

$$N_{\text{part}}^{\ell,V} = \frac{N_{\text{sig}}^{\ell,V}}{\epsilon_{\text{trig}}^\ell \times \epsilon^\ell \times C_V^\ell}. \quad (2)$$

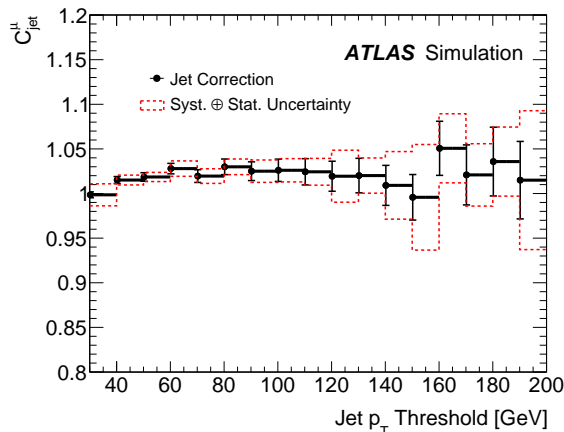


FIG. 1: Detector jet spectrum correction ( $C_{\text{jet}}^{\mu}$ ) on  $R_{\text{jet}}$  in the muon channel derived from ALPGEN. The uncertainty, shown as a dashed red line accounts for the difference between PYTHIA and ALPGEN generators. The black error bars show the statistical uncertainty alone.

where the boson corrections  $C_V^{\ell}$  correct the observed phase space to the truth (particle) level kinematic phase space, accounting for the resolution of leptons and  $E_T^{\text{miss}}$ .

Trigger and identification efficiency for leptons were determined from an unbiased control sample by selecting a well identified “tag” lepton and a additional “probe” inner detector track in  $Z \rightarrow \ell\ell$  candidate events. The efficiency is the fraction of probe tracks matched to a reconstructed lepton and passing all identification requirements. These efficiencies were found to be largely independent of jet kinematics, other than through correlations with lepton kinematics due to the jet recoiling against the  $W$  or  $Z$ . Therefore, these efficiencies were binned in lepton  $p_T$  and  $\eta$  for the electron channel, and  $\eta$  and  $\phi$  for the muon channel, for all jet  $p_T$  thresholds.

When the ratio of cross sections is measured, jet resolution and scale effects almost completely cancel. A correction  $C_{\text{jet}}^{\ell}$  was applied to take into account small differences. This correction is defined as the ratio between the  $R_{\text{jet}}$  value as a function of particle level jet  $p_T$  threshold and the  $R_{\text{jet}}$  value as a function of reconstructed jet  $p_T$  threshold. This factor is measured in simulation samples and applied as follows:

$$R_{\text{jet}} = \frac{N_{\text{part}}^{\ell, W}}{N_{\text{part}}^{\ell, Z}} \times C_{\text{jet}}^{\ell}. \quad (3)$$

This correction is shown for the muon channel in Figure 1. Differences from unity correspond to an offset in the amount of migration between jet  $p_T$  bins between  $W$ +jet and  $Z$ +jet events. This is mostly due to selection differences in the two channels before the jet selection, such as the requirement that the decay products be located in the detector volume. Note that binning in terms of jet  $p_T$  threshold eliminates migration across the upper bin edges.

## VII. SYSTEMATIC UNCERTAINTIES

In order to properly take into account correlations between the  $W$  and  $Z$  measurements, and to maximize cancellation of systematic uncertainties, all such uncertainties were measured as a relative change in  $R_{\text{jet}}$ . The total systematic uncertainty varies from 4% to 15%, generally increasing with increased jet  $p_T$  threshold. Systematic uncertainties on the measured ratio were divided into five broad groups: multijet background, electoweak background, boson reconstruction (combining  $\epsilon_{\text{trig}}^{\ell} \times \epsilon^{\ell} \times C_V^{\ell}$ ), the jet spectrum correction  $C_{\text{jet}}^{\ell}$ , and uncertainties related to generator differences, as shown in Figure 2.

Systematics on the multijet background were estimated by varying the parameters of each method, such as the selection of control samples used to derive the background fractions. Systematics on the electoweak background are estimated by varying the lepton identification criteria, by varying momentum scale and resolution, and by comparing samples generated with and without additional overlapping  $pp$  interactions.

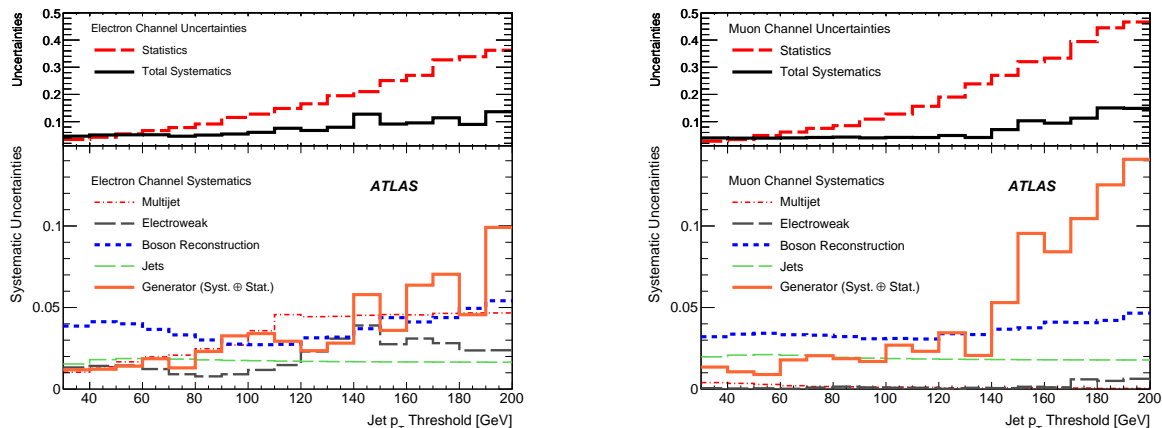


FIG. 2: Relative systematic uncertainties on  $R_{\text{jet}}$  in the electron channel (left) and in the muon channel (right). The top plot displays the total systematic and statistical uncertainty (shown as red dashed line) versus jet  $p_T$  threshold. The lower plot shows the breakdown of the systematic uncertainties. The “boson reconstruction” entry contains the uncertainties related to the leptons and  $E_T^{\text{miss}}$  (including trigger and lepton identification). The “jet” entry contains systematics of the jet correction as well as the jet energy scale and resolution. Uncertainties from each group were added in quadrature.

Boson reconstruction systematic uncertainties included those associated with identification and trigger efficiency, as well as scale and resolution effects. The single lepton trigger and identification efficiency uncertainties were derived using the methods documented in Ref. [8], and then propagated to uncertainties on  $R_{\text{jet}}$ . This leads to a total identification efficiency uncertainty of 1.1%(1.7%) for electrons (muons) independent of jet  $p_T$ . Trigger efficiency uncertainties were very small in both channels.

Uncertainties involving the scale of lepton momenta and  $E_T^{\text{miss}}$  were evaluated by directly scaling up and down the quantity in question by the measured scale uncertainty. In each case the deviation of  $R_{\text{jet}}$  was applied as a systematic uncertainty. Similarly, resolution effects were evaluated by smearing the quantities by a gaussian with the width of the measured resolution, repeating this process and taking the root mean squared deviation as the systematic uncertainty. Lepton momentum scale and resolution measurements and their uncertainties are determined by comparing the width and position of the invariant mass spectrum of Z candidates in data to that in a simulated sample.

Jet related systematics included those involved with jet energy scale (JES), jet energy resolution (JER) and their associated uncertainties. These quantities were determined from data and simulation comparisons [9]. The JES uncertainty includes components from calibration and jet sample composition differences. The JES calibration uncertainty varies with  $|\eta|$  and  $p_T$ , and ranges from 4% to 8%. The JES and JER were measured with di-jet events, which have different proportions of quark and gluon initiated jets than events containing vector bosons. Therefore, an uncertainty was assigned to account for the difference in calorimeter response between jets in  $V + \text{jet}$  events and the di-jet events used for calibration, ranging from 2 to 5%, and was added in quadrature to the JES calibration uncertainty. The total JES uncertainty ranges from approximately 10% at 20 GeV to 5% at 100 GeV. The JER is measured to vary from 2% at 20 GeV to 1% at 100 GeV. The uncertainties on  $R_{\text{jet}}$  due to JER and JES were evaluated using the same approach as for the lepton scale and resolution uncertainties. The uncertainties on  $R_{\text{jet}}$  due to the JER and JES were found to be approximately 0.5% and 2% respectively. This uncertainty includes a very small term to take into account the uncertainty on JER itself.

Jet related systematics also included the dominant uncertainty related to multiple pp collisions, the uncertainty of the efficiency of the JVF algorithm. Applying this algorithm to simulation with multiple interactions was found to produce consistent results with simulation not including additional interactions. The residual difference on  $R_{\text{jet}}$  between these cases was used as a systematic uncertainty on  $C_{\text{jet}}^\ell$ .

To account for systematics associated with generator modeling, correction factors were computed with samples generated with PYTHIA instead of ALPGEN, and the observed difference was applied as a systematic uncertainty. Systematic uncertainties were assigned from this variation to the following corrections:  $(C_{\text{jet}}^\ell)$ , the boson reconstruction correction  $C_V^\ell$ , and the electroweak background estimation  $f_{\text{ewk}}$ . At large jet  $p_T$  threshold, where the statistical uncertainty on the measurement dominates the total uncertainty, this systematic uncertainty is limited in statistical precision due to the size of the samples used, and is the dominant systematic uncertainty.

Systematic uncertainties were also estimated on the theoretical prediction. As our NLO parton-level calculation does not include the effects of hadronisation and underlying event, a correction was computed using PYTHIA as a function of jet  $p_T$  threshold. The uncertainty on this correction was evaluated by observing the effect of various generator tunes on the final  $R_{\text{jet}}$  result. These tunes increased or decreased the amount of underlying event, or varied the parameters controlling initial and final state radiation. Renormalization and factorization scale uncertainties were also included in our systematic uncertainties, as were PDF uncertainties.

### VIII. RESULTS

The ratio  $R_{\text{jet}}$  was measured in the fiducial region of the ATLAS detector as a function of jet  $p_T$  threshold, and corrected for detector effects. The electron and muon measurements were performed in slightly different phase space, due to the different  $\eta$  range and electron-jet isolation requirements, as well as for the different QED treatment between electron and muon definitions. The observed signal yields were corrected to recover the yield at particle level as described in Section VI.

The corrected ratio  $R_{\text{jet}}$  of the production cross sections in the leptonic (electron or muon) decays of the gauge bosons  $W$  and  $Z$  in association with exactly one jet is shown in Figure 3 as a function of the jet  $p_T$  threshold for the electron (left) and muon (right) channels. As the jet  $p_T$  threshold increases, the ratio  $R_{\text{jet}}$  is expected to decrease as the effective scale of the interaction becomes large compared to the difference in boson masses. This dependence is observed in the data. The values for the lowest jet  $p_T$  threshold of 30 GeV are:

$$R_{\text{jet}}(e) = 8.73 \pm 0.30 \text{ (stat)} \pm 0.40 \text{ (syst)}$$

$$R_{\text{jet}}(\mu) = 8.49 \pm 0.23 \text{ (stat)} \pm 0.33 \text{ (syst)}$$

Statistical uncertainties were evaluated by repeating the measurement with Monte Carlo pseudo-experiments assuming Poisson distributed data with a mean at the observed yield. Both electron and muon channel results are individually compatible with the theoretical predictions.

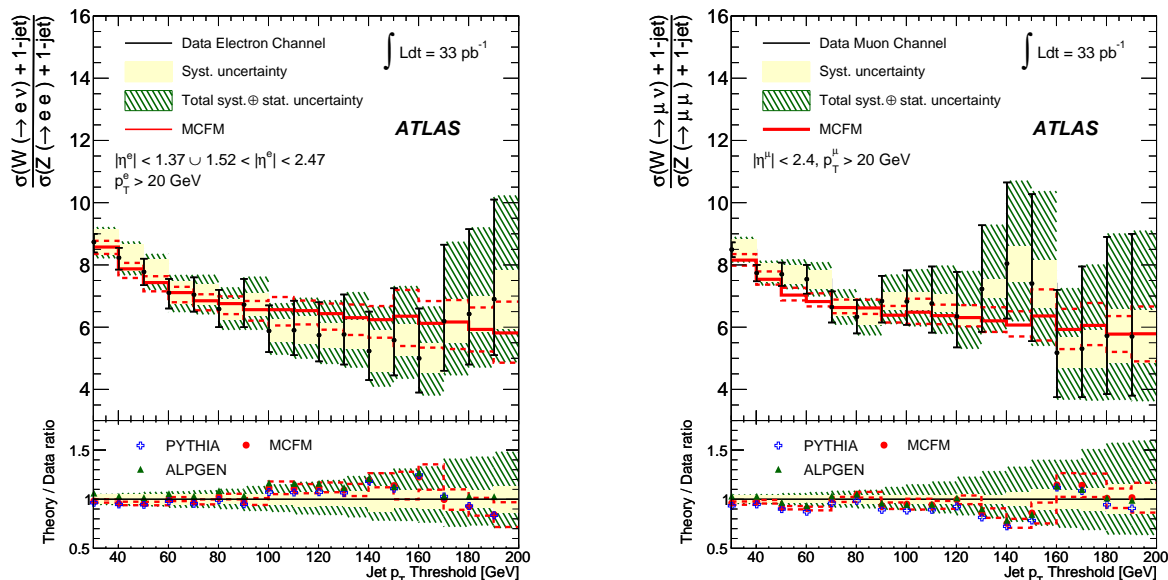


FIG. 3: Results for  $R_{\text{jet}}$  in the electron channel (left) and in the muon channel (right) for their respective fiducial regions. The results are compared to NLO predictions from MCFM (corrected to particle level using PYTHIA). Data are shown as black points at the lower bin edge corresponding to the jet  $p_T$  threshold with black error bars indicating the statistical uncertainties. The yellow band shows all systematic uncertainties added in quadrature and the green band shows statistical and systematic uncertainties added in quadrature. The theory uncertainty (dashed line) shown on the MCFM prediction includes uncertainties from PDF and renormalization and factorization scales. Note that these threshold data and their associated uncertainties are correlated between bins.

Electron and muon channel results were found to be compatible and therefore combined to reduce the statistical and uncorrelated systematic uncertainties on the result. Each channel was extrapolated to a common phase space, defined as  $|\eta_\ell| < 2.5$  before any QED radiation (Born level) with PYTHIA. The electron channel was further corrected for the effect of the electron-jet isolation requirements on the acceptance. This extrapolation to a common fiducial region decreases the value of the ratio for both channels primarily due to the more central distribution of leptons from the Z. The results were combined using a Bayesian approach [10] in the combination of systematic uncertainties accounting for correlations between them. The systematic uncertainties from  $E_T^{\text{miss}}$ , jet energy scale and resolution and electroweak background sources were considered fully correlated between the electron and muon channels. The combined result is shown in Figure 4 (left). The value of  $R_{\text{jet}}$  for the lowest jet  $p_T$  threshold of 30 GeV was found to be  $8.29 \pm 0.18$  (stat)  $\pm 0.28$  (syst). This combined measurement was also extrapolated to the full phase space, as shown in Figure 4 (right). For a jet  $p_T$  threshold of 30 GeV this ratio was found to be  $10.13 \pm 0.22$  (stat)  $\pm 0.45$  (syst).

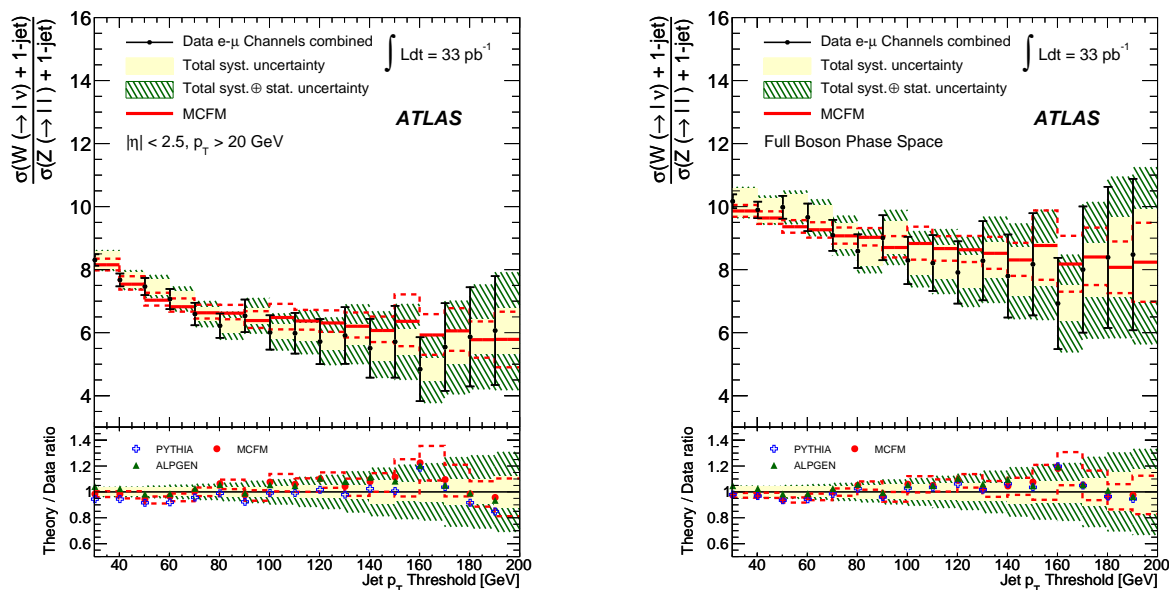


FIG. 4: Left: Combined electron and muon results for  $R_{\text{jet}}$  in a common fiducial region. The results are compared to predictions from MCFM (corrected to particle level). Data are shown with black error bars indicating the statistical uncertainties. The yellow band shows all systematic uncertainties added in quadrature and the green band shows statistical and systematic uncertainties added in quadrature. The theory uncertainty (dashed line) includes contributions from PDF and renormalisation and factorization scales. Right: Combined electron and muon results for  $R_{\text{jet}}$  extrapolated to the total phase space. Note that these threshold data and their associated uncertainties are correlated between bins.

## IX. SUMMARY

We present a measurement of the ratio of the production cross sections of the gauge bosons  $W$  and  $Z$  in association with exactly one jet, as a function of jet  $p_T$  threshold. This ratio was measured in fiducial phase space of the detector separately for muons and electrons. These results were also extrapolated to a common phase space and combined, as well as extrapolated to be the full phase space of the boson decay products. These results were provided as a function of jet  $p_T$  threshold from 30 to 200 GeV, exploring the transition region of electroweak scale breaking in perturbative jet production. The accepted theoretical model was found to be consistent with all results. This measurement has the advantage of having reduced theoretical and experimental systematic uncertainties due to correlations between the  $W$  and  $Z$  processes. This measurement builds the foundations of a high precision test of the Standard Model, and provides model-independent sensitivity to new physics coupling to leptons and jets. Comparisons with LO and NLO perturbative QCD predictions were made and found to be in agreement with data over the jet  $p_T$  threshold range covered by this measurement.

- [1] ATLAS Collaboration, arXiv:1108.4908[hep-ex] (2011).
- [2] M. Cacciari, G. P. Salam, and G. Soyez, *J. High Energy Phys.* **0804**, 063 (2008).
- [3] ATLAS Collaboration, *J. Instrum.* **3**, S08003 (2008).
- [4] M. L. Mangano et al., *J. High Energy Phys.* **0307**, 001 (2003).
- [5] T. Sjöstrand, S. Mrenna, and P. Skands, *J. High Energy Phys.* **0605**, 026 (2006).
- [6] S. Frixione, P. Nason, and C. Oleari, *J. High Energy Phys.* **0711**, 070 (2007).
- [7] S. Agostinelli et al., *Nucl. Instrum. Methods Phys. Res., Sect. A* **506**, 250 (2003).
- [8] ATLAS Collaboration, *JHEP* **1012**, 060 (2010), 1010.2130.
- [9] ATLAS Collaboration, *Eur. Phys. J. C* **71**, 1512 (2011).
- [10] A. C. Caldwell, D. Kollar, and K. Kroninger, *J. Phys. Conf. Ser.* **219**, 032013 (2010).